CD47 blockade reduces the pathologic features of experimental cerebral malaria and promotes survival of hosts with *Plasmodium* infection

Laughing Bear Torrez Dulgeroff[a,1], Miranda S. Oakley[b], Michal C. Tal[a], Ying Ying Yiu[a], Joy Q. He[a], Maia Shoham[a], Victoria Majam[b], Winter A. Okoth[b], Pallavi Malla[b], Sanjai Kumar[b], and Irving L. Weissman[a,1]

[a]Institute for Stem Cell Biology and Regenerative Medicine, Stanford University School of Medicine, Stanford, CA 94305; and [b]Laboratory of Emerging Pathogens, Division of Emerging and Transfusion Transmitted Diseases, Office of Blood Research and Review, Center for Biologics Evaluation and Research, Food and Drug Administration, Silver Spring, MD 20993

Contributed by Irving L. Weissman, January 28, 2021 (sent for review June 24, 2019; reviewed by Jay A. Berzofsky and Christian Engwerda)

CD47 is an antiphagocytic "don't eat me" signal that inhibits programmed cell removal of self. As red blood cells (RBCs) age they lose CD47 expression and become susceptible to programmed cell removal by macrophages. CD47$^{-/-}$ mice infected with *Plasmodium yoelii*, which exhibits an age-based preference for young RBCs, were previously demonstrated to be highly resistant to malaria infection. Our study sought to test the therapeutic benefit of CD47 blockade on ameliorating the clinical syndromes of experimental cerebral malaria (ECM), using the *Plasmodium berghei* ANKA (*Pb-A*) murine model. In vitro we tested the effect of anti-CD47 mAb on *Plasmodium*-infected RBC phagocytosis and found that anti-CD47 treatment significantly increased clearance of *Plasmodium*-infected RBCs. Infection of C57BL/6 mice with *Pb-A* is lethal and mice succumb to the clinical syndromes of CM between days 6 and 10 postinfection. Strikingly, treatment with anti-CD47 resulted in increased survival during the cerebral phase of *Pb-A* infection. Anti-CD47–treated mice had increased lymphocyte counts in the peripheral blood and increased circulating levels of IFN-γ, TNF-α, and IL-22. Despite increased circulating levels of inflammatory cytokines, anti-CD47–treated mice had reduced pathological features in the brain. Survival of ECM in anti-CD47–treated mice was correlated with reduced cellular accumulation in the cerebral vasculature, improved blood–brain barrier integrity, and reduced cytotoxic activity of infiltrating CD8$^+$ T cells. These results demonstrate the therapeutic benefit of anti-CD47 to reduce morbidity in a lethal model of ECM, which may have implications for preventing mortality in young African children who are the highest casualties of CM.

CD47 | *Plasmodium berghei* ANKA | cerebral malaria

Malaria remains a major public health challenge in developing countries. According to the World Health Organization (WHO), in 2018, there were an estimated 218 million cases and 405,000 malaria-related deaths. About 93% of these deaths were reported from the WHO African regions alone and were mostly caused by the most virulent form of human malaria, *Plasmodium falciparum* infections. Cerebral malaria (CM) is a major pathogenic consequence of *P. falciparum* infection and a leading cause of malaria deaths in African children under 5 y of age. Currently, there is no treatment available to suppress the clinical syndromes of CM and patient symptoms are managed by administration of antimalaria drugs to control parasitemia and supported by adjunct therapies including exchange transfusion (1).

CD47 is a 50-kDa transmembrane surface protein with an extracellular IgV domain that is ubiquitously expressed at varying levels across all cell types (2, 3). CD47 is a potent "don't eat me" signal regulating programed cell removal (PrCR) (4, 5). When CD47 binds to inhibitory receptor signal-regulatory protein-α (SIRPα), on the surface of phagocytic cells, the immunoreceptor tyrosine-based inhibitory motif within the cytoplasmic domain of SIRPα of phosphorylates tyrosine phosphatases SHP1/2, which inhibit the myosin assembly necessary for phagocytosis (6–8). CD47 is the predominant surface marker of red blood cell (RBC) turnover; newly produced RBCs have high surface expression of CD47, which degrades as a function of RBC age. The importance of CD47 expression on RBCs was demonstrated when labeled CD47 knockout cells were rapidly cleared after transplantation into wild-type mice. Furthermore, these studies used SIRPα antibodies to block phagocytosis in vitro and demonstrated that CD47, the ligand for the inhibitory receptor SIRPα, is critical to preventing PrCR of healthy RBCs (9, 10).

While blocking the interaction of CD47 is important for promoting phagocytosis, CD47 blockade alone is not sufficient and requires concurrent expression of a prophagocytic or "eat me" signal on the surface of the target cell (11). Subsequent studies identified cell surface expression of calreticulin (CRT) as the predominant prophagocytic signal that preferentially promotes phagocytosis of tumor cells while sparing healthy cells upon CD47 blockade (12). The role of CRT as a prophagocytic signal

Significance

Novel therapies are urgently needed that can ameliorate the clinical syndromes of cerebral malaria, the most severe consequences of *Plasmodium* infection, and thereby reduce malaria fatality. Monoclonal antibodies that target CD47, a "don't eat me" signal, have been demonstrated to enhance cellular clearance of cancer cells by promoting macrophage phagocytosis. We sought to adopt this therapeutic strategy to ameliorate the clinical syndromes associated with cerebral malaria with the goals of reducing disease-associated morbidity and mortality. We demonstrate that CD47 blockade by anti-CD47 injection leads to survival from cerebral malaria in mice.

Author contributions: L.B.T.D., S.K., and I.L.W. designed research; L.B.T.D., M.S.O., M.C.T., Y.Y.Y., J.Q.H., M.S., V.M., W.A.O., and P.M. performed research; L.B.T.D., M.S.O., and M.C.T. analyzed data; and L.B.T.D., S.K., and I.L.W. wrote the paper.

Reviewers: J.A.B., National Cancer Institute, NIH; and C.E., Queensland Institute of Medical Research.

Competing interest statement: I.L.W. is on patent applications from Stanford on the use of CD47 blocking agents in infectious disease. He was also cofounder, director, stockholder, and consultant in the company Forty Seven, Inc., which was purchased by Gilead, Inc., a company in which he has no consulting or financial role or agreements. As cofounder, I.L.W. has been asked to explain topics pursued by Forty Seven in the transition, but without financial compensation from or other agreements with Gilead currently.

[1]To whom correspondence may be addressed. Email: laughingbeartorrez@gmail.com or irv@stanford.edu.

This article contains supporting information online at https://www.pnas.org/lookup/suppl/doi:10.1073/pnas.1907653118/-/DCSupplemental.

Published March 8, 2021.

is intriguing in the context of transcriptionally silent enucleated RBCs, as activated macrophages have been demonstrated to secrete CRT that binds to asialoglycans on the surface of target cells, leading to macrophage CD91-mediated PrCR, and can thus act as a cell extrinsic prophagocytic signal (13, 14).

Previous reports have demonstrated that CD47 plays an important role in *Plasmodium* infection. During late-stage malaria infection (15 d postinfection) CD47 has been demonstrated to counterbalance high levels of phosphatidyl serine on both uninfected and infected RBCs the dynamics of which play an important role in malarial anemia (15). Experiments by Banerjee et al. (16) were the first to demonstrate that *Plasmodium yoelii*, which preferentially infects young RBCs that possess high expression of CD47, are protected from PrCR; this suggested that blockade of the CD47 "don't eat me" signal can provide therapeutic benefit in *Plasmodium* infection (16). Furthermore, disruption of SIRPα has been demonstrated to increase phagocytosis of *P. falciparum*-infected RBCs (17). In this study, we have investigated the therapeutic benefit of CD47 blockade on parasite burden and survival from the clinical syndromes of experimental CM (ECM) in mice caused by infection with *Plasmodium berghei* ANKA parasites. *P. berghei* ANKA (*Pb-A*) is a lethal model of severe malaria where infected mice succumb to ECM (C57BL/6 mice) or severe anemia (BALB/c mice). Our results show that CD47 blockade by injection of anti-CD47 mAb protected 80% of C57BL/6 mice against ECM and death.

Results

Treatment with Anti-CD47 Enhances Macrophage-Mediated PrCR of *Plasmodium*-Infected RBCs In Vitro. CD47 blockade alone is not sufficient to promote PrCR; there must be a prophagocytic signal on the surface of the target cell. We initiated our studies by examining the expression of prophagocytic signal CRT on the surface of RBCs from mice over the course of *Pb-A* infection in BALB/c mice. In this murine model of severe malaria, 100% of *Pb-A*–infected BALB/c mice develop lethal severe anemia and hyperparasitemia. Blood was collected from BALBc mice infected with 10^6 parasites of a transgenic strain of *Pb-A*, which constitutively expresses GFP, on days 0, 5, 10, 15, and 20 postinfection. Flow cytometry analysis was used to determine the percentage of CRT^+ parasitized RBCs (pRBCs) over the course of infection. A gradual but significant increase in the percentage of CRT^+ pRBCs was observed over the course of infection (Fig. 1*A*). Additionally, pRBCs from infected mice had significantly higher levels of CRT on their cell surface compared to RBCs from uninfected mice (Fig. 1*B*). Given the inherent transcriptional silence of mature RBCs, it is likely that prophagocytic CRT on the surface of RBCs over the course of malaria infection is achieved in a cell-extrinsic manner, likely by macrophage secretion as has been demonstrated previously (13).

We then determined whether CD47 expression on RBCs during *Plasmodium* infection prevents efficient cellular clearance by performing in vitro phagocytosis assays. We tested the effect of mouse anti-CD47 mAb, MIAP410, compared to IgG1 isotype, and PBS controls when RBCs from a *Pb-A*–infected mouse were coincubated with syngeneic mouse macrophages. Anti-CD47 treatment resulted in a 4.7-fold increase in pRBC phagocytosis, supporting the hypothesis that CD47 blockade in vivo may reduce parasite load and potentially reduce morbidity and mortality (Fig. 1*C*). In addition to mouse phagocytosis assays, we also tested the efficacy of human anti-CD47 mAb, Hu5F9G4, against *P. falciparum*–infected human RBCs. Similar to our observations in the mouse model, we found that CD47 blockade with Hu5F9G4 lead to a 2.3-fold increase in phagocytosis compared to the IgG4 isotype control (Fig. 1*D*). These results confirmed that CD47 blockade promotes PrCR of pRBCs in both murine and human in vitro models.

CD47 Blockade Promotes Survival of the Cerebral Phase of *Pb-A* Infection. To determine whether CD47 blockade could serve as a promising therapeutic against CM, we measured the effect of a single dose of anti-CD47 on susceptibility to ECM in the *Pb-A* murine model. In this murine model of ECM, C57BL/6 mice develop symptoms that resemble the clinical features of human CM during the cerebral phase (days 6 to 10) of infection. Mice that do not develop ECM will instead develop severe anemia and hyperparasitemia after day 15 postinfection, which is also lethal. C57BL/6 mice infected with 10^6 *Pb-A* parasites were treated with either PBS or MIAP410, an anti-CD47 monoclonal antibody (mAb), on day 3 postinfection and susceptibility to ECM, as well as peripheral parasitemia, was compared. We found that 100% of PBS-treated mice developed ECM and succumbed 6 to 9 d postinfection. Conversely, 80% of the MAIP410-treated mice did not develop ECM and survived the cerebral phase of infection (Fig. 2*A*). On day 5 postinfection, PBS-treated mice had 3.1% parasitemia compared to MIAP410-treated mice, which had 2.2% parasitemia (Fig. 2*B*). There was no significant difference in peripheral parasitemia during the cerebral phase of infection (*SI Appendix*, Fig. S1). Furthermore, MIAP410-treated mice that developed ECM compared to MIAP410-treated mice that did not develop ECM could not be predicted based on parasitemia.

To determine if anti-CD47–mediated PrCR is involved in the prevention of ECM, C57BL/6 mice were treated three times a week with 400 μg of anti-colony-stimulating factor 1 receptor (CSF1R) 2 wk prior to and throughout the course of *Pb-A* infection in order to deplete resident monocytes and macrophages. Depleted mice were infected with 10^6 *Pb-A* parasites and treated with either PBS or MIAP410 on day 3 postinfection and susceptibility to ECM, as well as peripheral parasitemia was compared. Despite long-term macrophage depletion, MIAP410-treated mice had reduced susceptibility to ECM and had similar survival rates to MIAP410-treated mice that had not received anti-CSF1R depletion (Fig. 2 *C* and *D* and *SI Appendix*, Fig. S2). These data suggest that while anti-CD47 treatment enhanced PrCR in vitro, in vivo survival of ECM is independent of the regulatory role of CD47 on RBC clearance, or at least by the anti-CSF1R–depleted phagocytes.

CD47 Blockade Results in a More Productive but Less Pathologic Immune Response in Blood. Complete blood counts (CBC) were used to evaluate the effect of anti-CD47 treatment on peripheral blood during *Pb-A* infection. *Pb-A*–infected mice were treated with PBS or MIAP410 on day 3 postinfection and their blood was examined at the onset of the cerebral phase of infection on day 6. On day 6 postinfection, PBS- and MIAP410-treated mice had minimal signs of anemia. MIAP410-treated mice had 6.8×10^6 RBC/μL and PBS-treated mice had 7.5×10^6 RBC/μL, as well as comparable level of parasitemia (Fig. 3 *A* and *B*). There was also minimal difference between PBS compared to MIAP410-treated mice for additional RBC parameters; hemoglobin (11.9 g/dL vs. 10.5 g/dL), hematocrit (41.9% vs. 37.0%), mean corpuscular volume (55.7 fL vs. 54.6 fL), and mean corpuscular hemoglobin concentration (15.8 g/dL vs. 15.6 g/dL). These levels of drop in red cell parameters, ∼10%, are comparable to data in nonhuman primates and humans after the first dose of blocking anti-CD47 antibodies (18). These results demonstrate that anti-CD47 treatment minimally impacts RBC parameters, nor does it exacerbate anemia (Fig. 3*A*). There was a 1.8-fold increase in circulating white blood cells (WBC) in MIAP410-treated mice compared to PBS-treated mice (Fig. 3*A*). Specifically, MIAP410-treated mice had a 1.9-fold increase in circulating lymphocytes compared to PBS-treated mice, whereas there was no significant difference in circulating neutrophils, monocytes, or eosinophils (Fig. 3*C*). To further investigate the anti-CD47–mediated inflammatory response to *Pb-A* during the cerebral phase of

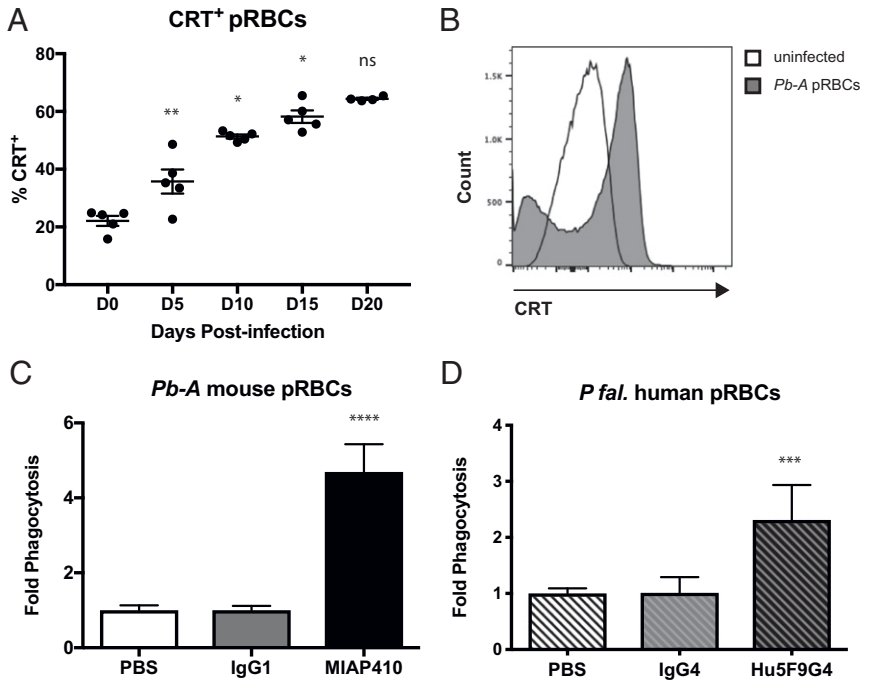

Fig. 1. Anti-CD47 treatment enhances programmed cell removal of *Plasmodium*-infected RBCs in vitro. (*A*) Percent CRT$^+$ pRBCs isolated from *Pb-A*-GFP infected BALB/c mice on days 0, 5, 10, 15, and 20 postinfection (*$P < 0.05$, **$P < 0.01$; ns, not significant). (*B*) Representative histogram of CRT surface expression on TER119$^+$ RBCs from an uninfected mouse (white) and TER119$^+$GFP$^+$ pRBCs from *Pb-A*–infected mouse day 20 postinfection. (*C*) Ter119$^+$GFP$^+$ *Pb-A* pRBCs were enriched by FACS and coincubated with syngeneic mouse macrophages following treatment with anti-CD47 mAb (MIAP410) compared to IgG1 isotype and PBS vehicle controls. Fold-change phagocytosis was determined by FACS analysis of GFP$^+$ macrophages across treatments compared to PBS control (****$P < 0.0001$). (*D*) *P. falciparum* isolate 2D3-GFP$^+$ human pRBCs were enriched by FACS and coincubated with human macrophages in the presence of anti-CD47 mAb (Hu5F9G4) compared to IgG4 isotype and PBS vehicle controls (***$P < 0.0009$).

infection, serum was collected from the same mice on day 6 postinfection with *Pb-A* for Luminex cytokine and chemokine profiling. Of the 39 cytokines and chemokines measured, three were significantly up-regulated by MIAP410-treated mice: interferon (IFN)-γ, tumor necrosis factor (TNF)-α, and interleukin (IL)-22 (Fig. 3*D* and *SI Appendix*, Fig. S3). The cytokine profile of the anti-CD47–treated mice along with their increased circulating leukocytes suggests that blockade promotes a shift toward a more inflammatory immune response to *Pb-A* infection.

CD47 Blockade Preserves Blood–Brain Barrier Integrity and Prevents ECM. The pathology of ECM is characterized by neurological symptoms, coma, and death, proposed to result from inflammation-induced cellular retention or accumulation within the cerebral vasculature and dysfunction of the blood–brain barrier (19). On day 6 postinfection, 100% of PBS-treated mice had succumbed to ECM or had reached morbidity end-point criteria. Conversely, MIAP410-treated mice showed no symptoms of ECM and 100% of cage mates not euthanized for histopathology survived the cerebral phase of infection. We compared histopathology of MIAP410-treated and PBS-treated mice by H&E staining of paraffin-embedded tissues from all major organs during the cerebral phase (day 6) of *Pb-A* infection. Most strikingly, MIAP410-treated mice had reduced cellular accumulation in the brain compared to PBS-treated mice, which had increased leukocytes surrounding the meningeal vessels, within the brain blood vessel lumen, and within the Virchow Robins space (Fig. 4 *A–D*). Furthermore, PBS-treated mice exhibited decimated meningeal architecture, whereas MIAP410-treated mice had intact meningeal architecture. One of the PBS-treated mice was so severely affected by the clinical syndromes of ECM that histopathologic examination revealed a hemorrhage (black arrowhead in *SI Appendix*, Fig. S4*B*) within the interstitium of the spinal cord, whereas no lesions were observed in the MIP410-treated mice (*SI Appendix*, Fig. S4). Reduced cellular accumulation was also observed in the liver of the MIAP410-treated mice compared to PBS-treated controls, possessing decreased RBCs and WBCs within the liver parenchyma and blood vessel lumen. Additionally, there was reduced observation of *Plasmodium* metabolite hemozoin (represented by black arrowheads in *SI Appendix*, Fig. S5) within the tissue of MIAP410-treated mice compared to PBS-treated mice.

The histopathology in the brain and other tissues demonstrated that mice treated with MIAP410 lacked the cellular accumulation observed as a result of *Pb-A* infection in PBS-treated controls, suggesting anti-CD47–treated mice maintained vascular functionality. An Evans blue permeability assay was used to measure blood–brain barrier integrity, Evans blue is an intravital dye that binds to albumin, which does not cross the blood–brain barrier under normal conditions (20). MIAP410-treated, PBS-treated, or uninfected control mice were injected with 2 mL/kg 2% Evans blue 30 min prior to being euthanized on day 6 postinfection. Brains were then harvested, imaged, processed, and the optical density (OD) of Evans blue dye within the brain was measured at 620 nm by absorbance plate reader (Fig. 4*E*). As expected, PBS-treated mice had increased levels of Evans blue in the brain, confirming that the *Pb-A*–infected PBS-treated mice experience severe effects of CM, specifically vascular leakage at the blood–brain barrier. However, CD47 blockade-treated mice had significantly lower levels of Evans blue in the brain, indicating that CD47 blockade protects the blood–brain barrier from vascular leakage (Fig. 4*F*).

CD47 Blockade Reduces CD8$^+$ T Cell Accumulation and Proinflammatory Response in the Brain during ECM. To examine the effect of CD47 blockade on a cellular level, CD8$^+$ T cells

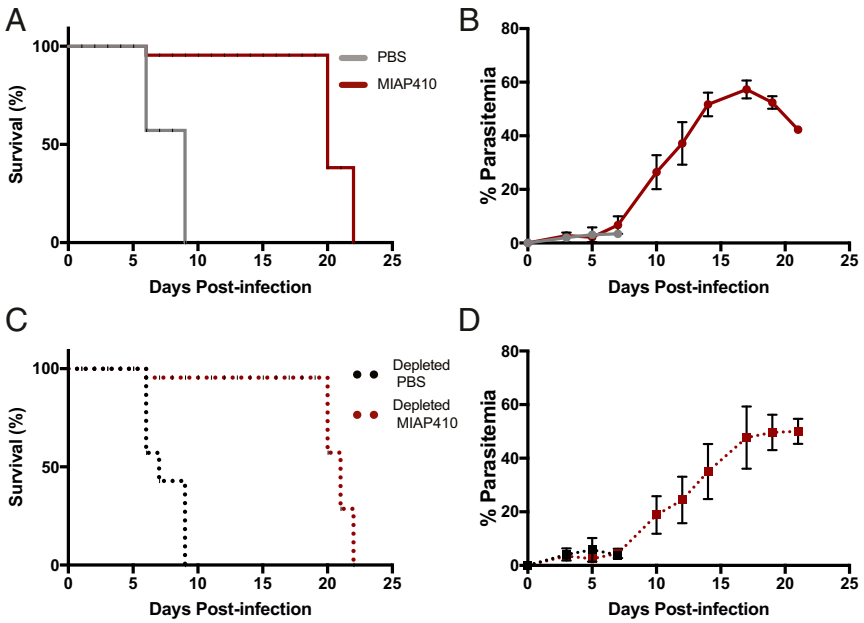

Fig. 2. CD47 blockade-treated mice survive the cerebral phase of *Pb-A* infection. (*A*) *Pb-A* infection survival curves of PBS and anti-CD47–treated (MIAP410) mice. Cerebral phase of infection is 6 to 10 d postinfection. (*B*) Percent parasitemia over the course of *Pb-A* infection in C57BL/6 mice treated with PBS or anti-CD47 (MIAP410) plotted as mean ± SEM ($n = 5$). (*C*) *Pb-A* infection survival curves of PBS and anti-CD47 treated (MIAP410) macrophage-depleted mice. Depletion was achieved by established methods using anti-CSF1R for 2 wk prior to infection and was continued throughout the experiment. (*D*) Percent parasitemia over the course of *Pb-A* infection in macrophage-depleted C57BL/6 mice treated with PBS or anti-CD47 (MIAP410) plotted as mean ± SEM ($n = 5$).

within the brain of *Pb-A*–infected mice were characterized by flow cytometry. During the peak of *Pb-A* infection on day 6 mice were perfused and brains were harvested, disassociated, and analyzed by flow cytometry. While there was a subtle reduction in $CD8^+$ T cells that had migrated into the brain tissue of anti-CD47–treated mice compared to PBS-treated mice (Fig. 4*G*), significant differences were observed in $CD8^+$ T cell cytokine and granzyme production. $CD8^+$ T cells within the brain of anti-CD47–treated mice produced lower levels of Granzyme B and IFN-γ (Fig. 4 *H* and *I*) at the site of pathogenic consequences of ECM. In summary, treatment with anti-CD47 reduced the severity of several events implicated in the pathogenesis of CM—cellular accumulation within the cerebral vasculature, breakdown of the blood–brain barrier, and $CD8^+$ T cell cytotoxicity within the brain—promoting survival of *Pb-A* infection.

Discussion

Abundant expression of CD47 across the hematopoietic lineage makes CD47 blockade a potential strategy to modulate the immune system. Several studies have demonstrated the broad utility of CD47 blockade to promote innate immune cell clearance (21–24) and adaptive immune responses (25–27). A recent clinical trial has demonstrated the safety and efficacy of CD47 blockade with rituximab in relapsed, refractory (to rituximab and chemotherapy) non-Hodgkin's lymphoma patients with diffuse large B cell lymphoma and follicular lymphoma (28), and in myelodysplastic syndromes and elderly onset acute myeloid leukemia patients in combination with azacytidine (29). The specificity of anti-CD47 treatment is not limited to cancer cells and is applicable to any target cell type upon which endogenous CD47 levels may be counterbalancing prophagocytic signaling. Indeed, we were able to identify increased levels of the prophagocytic signal, CRT, on the surface of pRBCs (Fig. 1*A*). Furthermore, previous studies and our own in vitro data demonstrate that blockade of CD47 signaling results in increased phagocytosis of pRBCs (Fig. 1 *C* and *D*) (16, 17). Thus, we directly tested CD47 blockade as a therapeutic strategy against *Plasmodium* infection in the murine model of CM.

Initially we assumed that CD47 blockade would enhance PrCR of pRBCs leading to reduced parasite burden, as our in vitro data supported this hypothesis. However, we observed no significant difference in the peripheral parasitemia between PBS-treated mice and anti-CD47–treated mice during the cerebral phase of infection (*SI Appendix*, Fig. S1). Long-term depletion of macrophages sensitive to CSF1R antibodies also had no effect on parasitemia or treatment outcomes during the early phase of infection. Thus, while in vivo CD47 blockade conferred protection during the cerebral phase of malaria infection, it appears to do so in a CSF1R macrophage-independent manner (Fig. 2). There are several possible reasons why CD47 blockade did not significantly enhance PrCR in our in vivo model. First, macrophage depletion with anti-CSF1R is imperfect, although this method did lead to a significant reduction in splenic macrophages in these experiments (*SI Appendix*, Fig. S2); the expanding inflammatory monocyte subset is not targeted by this approach and could have some RBC clearance potential, or more likely, are responsible for the cerebral perivascular inflammation in the disease. Second, *Pb-A* infection in mice is highly fulminant and parasite replication dynamics may outcompete PrCR during the acute phase of infection. This is an important point to consider given the age-based susceptibility of different malaria parasites (30). Malaria species *Plasmodium vivax* exhibit RBC susceptibility age restriction and can only infect young RBCs and reticulocytes, while on the other extreme, *Plasmodium malariae* only infect older RBCs (31, 32). However, *P. falciparum* exhibits no restriction in age-based RBC susceptibility, a feature that is associated with higher parasite burden and disease severity. Lack of restricted RBC targets permits species like *P. falciparum* and its mouse model *Pb-A* to possess distinct replication dynamics in comparison to more restricted strains of malaria. Since *Pb-A* infects both reticulocytes and mature cells, it is feasible that CD47 was less effective on

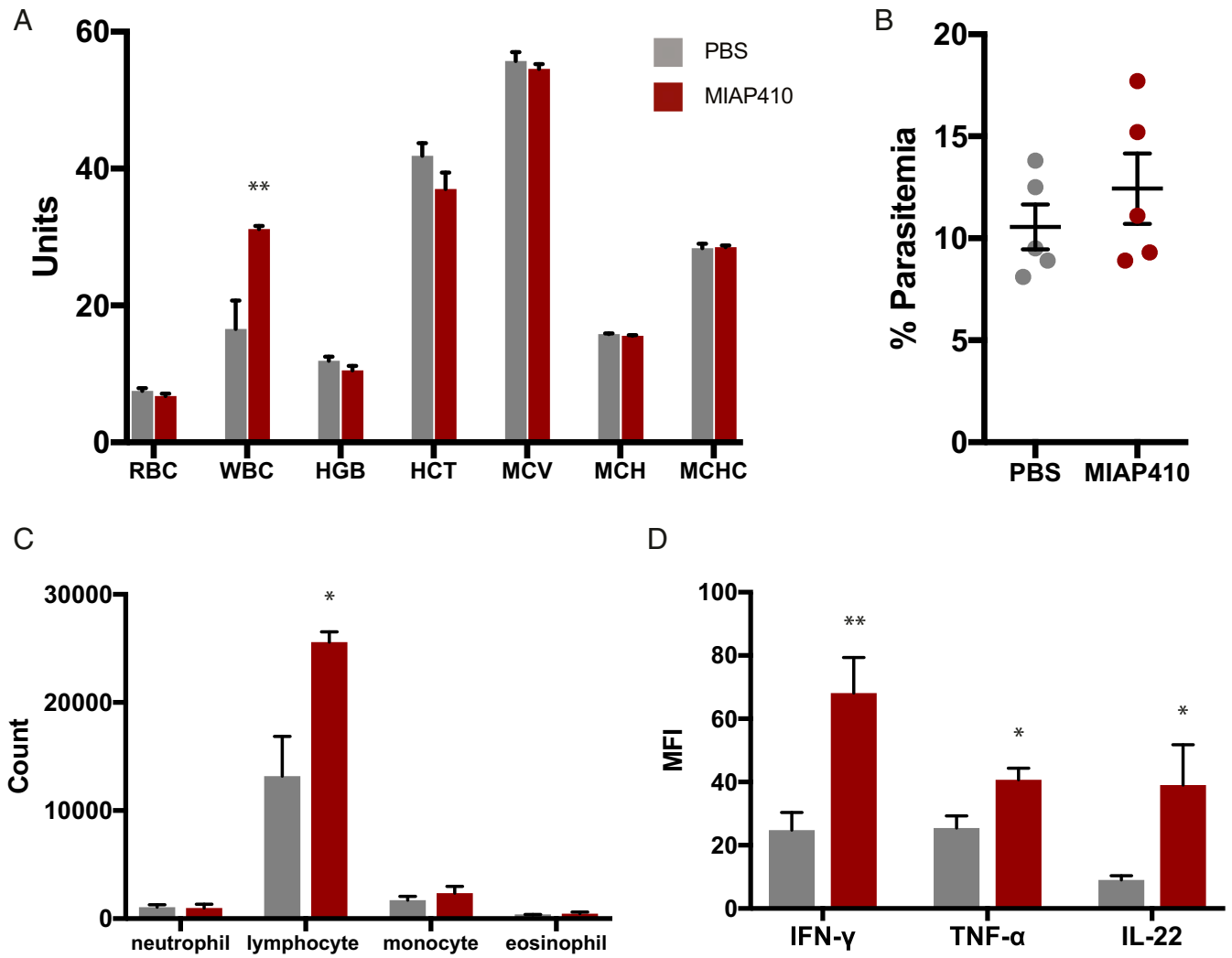

Fig. 3. Effects of CD47 blockade on peripheral blood of *Pb-A* infected C57BL/6 mice. (*A*) The following blood parameters were measured during the cerebral phase of infection on day 6 from PBS and anti-CD47 (MIAP410) -treated mice: red blood cells (RBC units = M/μL), white blood cells (WBC units = K/μL), hemoglobin (HGB units = g/dL), hematocrit (HCT units = %), mean corpuscular volume (MCV units = fL), mean corpuscular hemoglobin (MCH units in picograms), and mean corpuscular hemoglobin concentration (MCHC units in g/dL) (**$P < 0.01$). (*B*) Percent parasitemia of PBS and anti-CD47 (MIAP410) treated mice on day 6 postinfection. There was no significant difference in parasitemia. (*C*) Absolute count of WBC subsets (neutrophil, lymphocyte, monocyte, and eosinophil) were measured for during the cerebral phase of infection on day 6 from PBS and anti-CD47 (MIAP410) -treated mice (*$P < 0.05$). (*D*) Serum levels of IFN-γ, TNF-α, and IL-22 were measured by Luminex multiplex technology and are plotted as MFI ± SEM ($n = 5$) (*$P < 0.05$, **$P < 0.01$).

clearance of mature infected RBCs and parasite growth continued unabated.

The precise mechanisms of CM remain poorly understood. Previous studies of CM have shown that the host immune response is more indicative of the development of CM than peripheral parasitemia (33). This is supported by the fact that the WHO definition of *P. falciparum* hyperparasitemia varies across transmission areas and over time and is not a stable predictor of severe malaria (34). Similarly, we observed that despite similar levels of parasitemia, CD47 blockade significantly prevented mortality of CM in the *Pb-A* C57BL/6 murine model. Surprisingly, quantification of peripheral WBCs revealed that CD47 blockade led to an increase in circulating leukocytes, most of which were lymphocytes. Moreover, serum levels of proinflammatory cytokines IFN-γ and TNF-α, as well as IL-22, were increased following CD47 blockade (Fig. 3). Previous studies have demonstrated increased IFN-γ production following CD47 blockade (25). These data are intriguing given the important and complicated role of IFN-γ in the pathogenesis of ECM (35). It is also possible that IL-22, a member of the regulatory cytokine IL-10 family, previously reported to be protective in ECM (36), may ameliorate the observed proinflammatory response. While complex immune distinctions between anti-CD47–treated and PBS-treated mice were observed in the circulation, these results should be considered in the context of cellular and cytokine levels during the pathogenesis of ECM in the brain.

CD47 blockade ameliorated several fundamental and interconnected hallmarks of ECM (Fig. 4). Histopathological examination revealed a reduction in cellular accumulation and maintenance of vascular architecture in the brain. Evans blue assay confirmed that CD47 blockade treatment reduced the impairment of the blood–brain barrier associated with CM. The reduced occurrence of CM observed with administration of anti-CD47 likely involves complex pathways that result in prevention of cerebral perivascular accumulations of leukocytes, perhaps secondary to reduced stimulus to cause them to accumulate in

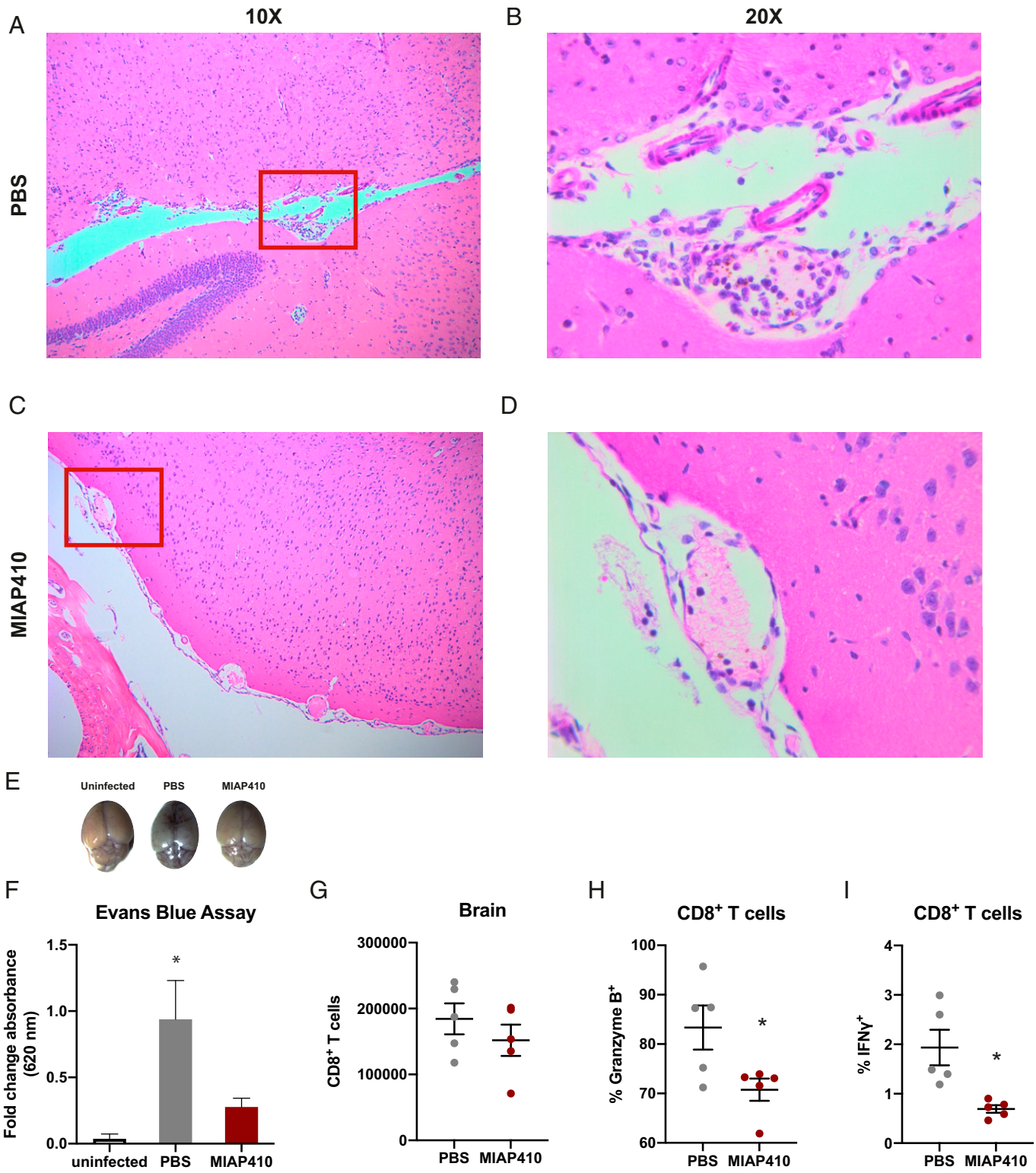

Fig. 4. CD47 blockade reduces pathologic features of ECM. (*A*) H&E staining of brain tissue of PBS treated C57BL/6 mice on day 6 postinfection with *Pb-A* taken at 10× and (*B*) 20×, compared to (*C*) anti-CD47 treated mice taken at 10× and (*D*) 20×. Red box represents field of view for 20× magnification. (*E*) Representative images of brains following Evans blue permeability assay, to measure blood–brain barrier integrity, of C57BL/6 mice on day 6 postinfection treated with PBS, anti-CD47 (MIAP410) compared to an uninfected control. (*F*) Quantification of blood–brain barrier permeability represented as fold-change absorbance (OD_{620}) over uninfected controls. (*G*) FACS quantification of $CD8^+$ T cells located within the perfused brain tissue of C57BL/6 mice on day 6 postinfection with *Pb-A* from PBS or anti-CD47 (MIAP410)-treated mice. (*H*) Percent of Granzyme B^+ $CD8^+$ T cells. (*I*) Percent of IFN-γ^+ $CD8^+$ T cells. ($n = 5$) (*$P < 0.05$).

these vessels. These distinctions are also potentially integral to the activation of $CD8^+$ T cells, which play a central role in the pathogenesis of CM (37). *Pb-A* infection is associated with increased cellular accumulation and cross-presentation to $CD8^+$ T cells, leading to migration into the perivascular spaces within the brain microvasculature. Perivascular APCs, presenting parasite antigen as a result of reduced blood–brain barrier integrity, prime $CD8^+$ T cells, which upon activation release cytokines and cytotoxic granules. CD47 blockade was demonstrated to reduce cellular accumulation in the brain and improve the integrity of the blood–brain barrier during *Pb-A* infection, which were correlated to a reduction in $CD8^+$ T cell cytotoxicity.

Although we initially hypothesized that CD47 blockade would enhance PrCR and attenuate disease burden by reducing parasitemia, we found that CD47 blockade reduced morbidity of ECM through reducing the cytotoxicity of leukocyte infiltration within the brain that is directly associated with disease pathogenesis. While it is difficult to determine the precise order of events that prevent ECM, given the ubiquity of CD47 expression and complexity of ECM pathology, the effects of CD47 on $CD8^+$ T cell cytotoxicity warrant further investigation. Our study represents a foundation for preclinical and clinical studies to investigate the prospect of anti-CD47 mAb administration to reduce morbidity and mortality in CM patients, particularly in young African children.

Materials and Methods

Mice, Parasites, and Infection. Age-matched female C57BL/6 or BALB/c mice were obtained from The Jackson Laboratory. Mice from the I.L.W. laboratory at Stanford University were maintained in the Stem Cell Institute and experiments were carried out in accordance with guidelines set by the Stanford University Administrative Panel on Laboratory Animal Care (Animal Study Protocol 30109). Mice from the S.K. laboratory at the Food and Drug Administration (FDA) were maintained at the facilities at the Center for Biologics Evaluation and Research and experiments were carried out in accordance with the guidelines set forth for the care and use of laboratory animals by the FDA (Animal Study Protocol 2002-21). *Pb-A*, *Pb-A* GFPCON 259cl2 obtained through BEI Resources, was used as the source of parasite infection in both in vitro and in vivo experiments. Mice were infected by intraperitoneal injection of 10^6 pRBCs from a donor mouse. Water for donor mice was treated with 0.07 mg/mL pyrimethamine to select for GFP^+ parasites.

CRT Expression. To determine the expression of CRT, mice were bled and whole blood was stained with anti-CRT mAb (FMC 75) conjugated to phycoerythrin (PE) and Ter119 (Ly-76) conjugated to Alexa Fluor 700. pRBCs were gated as $Ter119^+GFP^+$ and the percent CRT^+ pRBCs and median fluorescent intensity (MFI) were measured on an LSR Fortessa.

Phagocytosis Assays of RBCs by Mouse Bone Marrow-Derived Macrophages.
Macrophage derivation. Bone marrow-derived mouse macrophages were generated by performing a bone marrow flush of the tibia and femur of BALB/c mice that were 6 to 12 wk old. Bone marrow cells were mechanically dissociated and treated with ACK lysis buffer for 5 min. Cells were then differentiated in Iscove modified Dulbecco media + 10% FBS + 10 ng/mL mouse macrophage colony stimulating factor for 6 to 8 d. Peripheral blood-derived human macrophages were generated by Ficoll enrichment of white blood cells from peripheral blood (Leukocyte Reduction System Chambers of donor blood were purchased from the Stanford Blood Center). Cells were treated with ACK lysis buffer for 5 min and then adherence selection for 30 min and cultured in RPMI + 10% human serum for 6 to 9 d.

Target cell isolation. Mouse pRBCs were purified from BLABc mouse peripheral blood infected with *Pb-A* GFPCON 259cl2 by FACS. Human pRBCs were purified from type O donor blood infected in vitro with *P. falciparum* 3D7HT-GFP (courtesy of the Yeh laboratory at Stanford University, California, strain from BEI resources) using magnetic isolation with MACS columns (Miltenyi Biotech).

Phagocytosis Assays of RBCs by Human Monocyte-Derived Macrophages. Derived macrophages were harvested and counted by hemocytometer. Once purified, target cells were stained with carboxyfluorescein diacetate succinimidyl ester (CFSE) to enhance target cell signal strength and then counted. Target cells were cocultured with macrophages at a ratio of 2:1 for 1 h in the indicated treatment condition. CD47 blockade in vitro was achieved using anti-CD47 mAb, for mice MIAP410 (Bio X Cell) was used and for human Hu5F9G4 (Lonza) was used. Isotype control treatment for mouse was IgG1 isotype control (Bio X Cell) and for human was Ultra-LEAF purified IgG4 isotype control (BioLegend). Mouse macrophages were labeled with anti-mouse F4/80 (BioLegend), human macrophages were labeled with anti-human Macrophage Marker (eBioscience). Percent phagocytosis ($CFSE^+$ Macrophages) was quantified by FACS and normalized to PBS control to calculate fold-change in phagocytosis across treatment conditions.

In Vivo Mouse Treatments.
CD47 blockade. C57BL/6 mice were injected intraperitoneally with 100 μg of anti-CD47 MIAP410 (Bio X Cell) in 0.1 mL of phosphate buffered saline solution. Mice were treated with a single dose of anti-CD47 on day 3 postinfection unless otherwise noted.
Long-term macrophage depletion. Mice were treated injected intraperitoneally with 400 μg of anti-CSF1R (Bio X Cell) in 0.1 mL of phosphate buffered saline solution. Depletion began 2 wk prior to infection with *Pb-A*, mice were treated three times a week, and continued to receive treatment three times a week until experimental endpoints were reached.

Parasitemia and CBC. The peripheral parasitemia of experimental mice C57BL/6 mice was determined by FACS analysis. For FACS, 1 μL of blood was stained Ter119 (Ly-76) conjugated to Alexa Fluor 700 for 30 min and then diluted in 500 μL of FACS buffer (phosphate buffered saline solution + 2% FBS) for analysis. Peripheral parasitemia was measured as the percent of $Ter119^+$ RBCs that were *Pb-A*–GFP^+, parasitemia was also confirmed by microscopy on Giemsa-stained thin blood films. CBC were performed on the Sysmex XT-2000iV analyzer system and confirmed by blood smears analysis prepared with Wright–Giemsa stain.

Luminex. This assay was performed in the Human Immune Monitoring Center at Stanford University. Mouse 38 plex kits were purchased from eBiosciences/Affymetrix and used according to the manufacturer's recommendations, with modifications as described below. Briefly, beads were added to a 96-well plate and washed in a Biotek ELx405 washer. Samples were added to the plate containing the mixed antibody-linked beads and incubated at room temperature for 1 h followed by overnight incubation at 4 °C with shaking. Cold and room temperature incubation steps were performed on an orbital shaker at 500 to 600 rpm. Following the overnight incubation, plates were washed in a Biotek ELx405 washer and then biotinylated detection antibody added for 75 min at room temperature with shaking. The plate was washed as above, and streptavidin-PE was added. After incubation for 30 min at room temperature, wash was performed as above and reading buffer was added to the wells. Each sample was measured in duplicate. Plates were read using a Luminex 200 instrument with a lower bound of 50 beads per sample per cytokine. Custom assay Control beads by Radix Biosolutions was added to all wells.

Immunohistochemistry. During the cerebral phase of infection, on day 6 postinfection, portions of all major organs were harvested from mice from each treatment group. Harvested tissues were fixed in 10% buffered neutral formalin, routinely processed, and embedded in paraffin for sectioning and staining. H&E staining was performed by the Animal Diagnostic Laboratory in the Department of Comparative Medicine at Stanford University. Paraffin-embedded sections were shipped to Histowiz for immunohistochemistry, CD11b (ab133357, clone EPR1344).

Evans Blue Permeability Assay. On day 6 postinfection with *Pb*-A, C57/BL6 mice treated with PBS or anti-CD47, as described above, were injected retro-orbitally with 2 mL/kg 2% Evans blue and euthanized 30 min postinjection of the dye. Brains were collected, rinsed with PBS, and imaged. Brains were then mechanically dissociated and incubated in formaldehyde for 20 h at 55 °C, Evans blue-infused supernatant was transferred to 96-well plate and OD_{620} was measured by absorbance plate reader.

Flow Cytometry Characterization of $CD8^+$ T Cells. On day 6 postinfection with *Pb*-A, C57/BL6 mice, treated with PBS or anti-CD47 as described above, were perfused and euthanized. Brains were harvested, weighted, and mechanically dissociated in MACS buffer (PBS, 2% FBS, 2 mM EDTA). Dissociated cells were counted and stained with the following antibodies: anti-CD3, anti-CD8, anti–IFN-γ, and anti-Granzyme B (BioLegend). Spleens were harvested, weighted, and mechanically dissociated in MACS buffer. Dissociated cells

were counted and stained for anti-CD3, anti-CD8, anti–IFN-γ, and anti–TNF-α (BioLegend).

Data Availability. All study data are included in the article and *SI Appendix*.

ACKNOWLEDGMENTS. We thank all members of the I.L.W. and S.K. laboratories for support and helpful discussions; Katie Amberg-Johnson and the Yeh laboratory at Stanford for providing *Plasmodium falciparum* 3D7 used in phagocytosis assays; Yael Rosenberg-Hasson and the staff of the Stanford Human Immune Monitoring Center for their technical expertise and for running the mouse Luminex assays; José G. Vilches-Moure for consulting on mouse pathology; and the Animal Diagnostic Laboratory in the Department of Comparative Medicine at Stanford University. The following reagents were obtained through BEI Resources, National Institute of Allergy and Infectious Diseases, NIH: *Plasmodium berghei*, strain (ANKA) GFPCON 259cl2, MRA 865, contributed by Chris J. Janse and Andrew P. Waters, and *Plasmodium falciparum*, strain 3D7HT-GFP, MRA-1029, contributed by A. Talman and R. Sinden. Research reported in this publication was supported by the Virginia and D. K. Ludwig Fund for Cancer Research, Robert J. Kleberg Jr. and Helen C. Kleberg Foundation, and Food and Drug Administration intramural research funding. L.B.T.D. was supported by the Stanford Diversifying Academia, Recruiting Excellence fellowship; M.C.T. and Y.Y.Y. were supported by the Stanford Immunology Training Grant 5T32AI007290; and M.C.T. was also supported by the NIH National Research Service Award 1 F32 AI124558-01. J.Q.H was supported by the National Cancer Institute National Research Service Award F30CA228215 and Stanford Medical Scientist Training Grant T32GM007365.

1. WHO, *World Malaria Report* (World Health Organization, 2018).
2. F. P. Lindberg, H. D. Gresham, E. Schwarz, E. J. Brown, Molecular cloning of integrin-associated protein: An immunoglobulin family member with multiple membrane-spanning domains implicated in alpha v beta 3-dependent ligand binding. *J. Cell Biol.* **123**, 485–496 (1993).
3. M. I. Reinhold *et al*., In vivo expression of alternatively spliced forms of integrin-associated protein (CD47). *J. Cell Sci.* **108**, 3419–3425 (1995).
4. S. Jaiswal *et al*., CD47 is upregulated on circulating hematopoietic stem cells and leukemia cells to avoid phagocytosis. *Cell* **138**, 271–285 (2009).
5. S. Jaiswal, M. P. Chao, R. Majeti, I. L. Weissman, Macrophages as mediators of tumor immunosurveillance. *Trends Immunol.* **31**, 212–219 (2010).
6. A. Veillette, E. Thibaudeau, S. Latour, High expression of inhibitory receptor SHPS-1 and its association with protein-tyrosine phosphatase SHP-1 in macrophages. *J. Biol. Chem.* **273**, 22719–22728 (1998).
7. Y. Fujioka *et al*., A novel membrane glycoprotein, SHPS-1, that binds the SH2-domain-containing protein tyrosine phosphatase SHP-2 in response to mitogens and cell adhesion. *Mol. Cell. Biol.* **16**, 6887–6899 (1996).
8. R. K. Tsai, D. E. Discher, Inhibition of "self" engulfment through deactivation of myosin-II at the phagocytic synapse between human cells. *J. Cell Biol.* **180**, 989–1003 (2008).
9. P.-A. Oldenborg *et al*., Role of CD47 as a marker of self on red blood cells. *Science* **288**, 2051–2054 (2000).
10. P. A. Oldenborg, H. D. Gresham, F. P. Lindberg, CD47-signal regulatory protein alpha (SIRPalpha) regulates Fcgamma and complement receptor-mediated phagocytosis. *J. Exp. Med.* **193**, 855–862 (2001).
11. R. Majeti *et al*., CD47 is an adverse prognostic factor and therapeutic antibody target on human acute myeloid leukemia stem cells. *Cell* **138**, 286–299 (2009).
12. M. P. Chao *et al*., Calreticulin is the dominant pro-phagocytic signal on multiple human cancers and is counterbalanced by CD47. *Sci. Transl. Med.* **2**, 63ra94 (2010).
13. M. Feng *et al*., Macrophages eat cancer cells using their own calreticulin as a guide: Roles of TLR and Btk. *Proc. Natl. Acad. Sci. U.S.A.* **112**, 2145–2150 (2015).
14. M. Feng *et al*., Programmed cell removal by calreticulin in tissue homeostasis and cancer. *Nat. Commun.* **9**, 3194 (2018).
15. C. Fernandez-Arias *et al*., Anti-self phosphatidylserine antibodies recognize uninfected erythrocytes promoting malarial anemia. *Cell Host Microbe* **19**, 194–203 (2016).
16. R. Banerjee, S. Khandelwal, Y. Kozakai, B. Sahu, S. Kumar, CD47 regulates the phagocytic clearance and replication of the Plasmodium yoelii malaria parasite. *Proc. Natl. Acad. Sci. U.S.A.* **112**, 3062–3067 (2015).
17. K. Ayi *et al*., CD47-SIRPα interactions regulate macrophage uptake of Plasmodium falciparum-infected erythrocytes and clearance of malaria in vivo. *Infect. Immun.*, IAI.01426-15 (2016).
18. J. Liu *et al*., Pre-clinical development of a humanized anti-CD47 antibody with anti-cancer therapeutic potential. *PLoS One* **10**, e0137345 (2015).
19. I. M. Medana, G. D. H. Turner, Human cerebral malaria and the blood-brain barrier. *Int. J. Parasitol.* **36**, 555–568 (2006).
20. O. Uyama *et al*., Quantitative evaluation of vascular permeability in the gerbil brain after transient ischemia using Evans blue fluorescence. *J. Cereb. Blood Flow Metab.* **8**, 282–284 (1988).
21. M. P. Chao *et al*., Anti-CD47 antibody synergizes with rituximab to promote phagocytosis and eradicate non-Hodgkin lymphoma. *Cell* **142**, 699–713 (2010).
22. S. B. Willingham *et al*., The CD47-signal regulatory protein alpha (SIRPa) interaction is a therapeutic target for human solid tumors. *Proc. Natl. Acad. Sci. U.S.A.* **109**, 6662–6667 (2012).
23. K. Weiskopf *et al*., CD47-blocking immunotherapies stimulate macrophage-mediated destruction of small-cell lung cancer. *J. Clin. Invest.* **126**, 2610–2620 (2016).
24. S. Gholamin *et al*., Disrupting the CD47-SIRPα anti-phagocytic axis by a humanized anti-CD47 antibody is an efficacious treatment for malignant pediatric brain tumors. *Sci. Transl. Med.* **9**, eaaf2968 (2017).
25. X. Liu *et al*., CD47 blockade triggers T cell-mediated destruction of immunogenic tumors. *Nat. Med.* **21**, 1209–1215 (2015).
26. D. Tseng *et al*., Anti-CD47 antibody-mediated phagocytosis of cancer by macrophages primes an effective antitumor T-cell response. *Proc. Natl. Acad. Sci. U.S.A.* **110**, 11103–11108 (2013).
27. M. N. McCracken, A. C. Cha, I. L. Weissman, Molecular pathways: Activating T cells after cancer cell phagocytosis from blockade of CD47 "don't eat me" signals. *Clin. Cancer Res.* **21**, 3597–3601 (2015).
28. R. Advani *et al*., CD47 blockade by Hu5F9-G4 and rituximab in non-Hodgkin's lymphoma. *N. Engl. J. Med.* **379**, 1711–1721 (2018).
29. M. P. Chao *et al*., Therapeutic targeting of the macrophage immune checkpoint CD47 in myeloid Malignancies. *Front. Oncol.* **9**, 1380 (2020).
30. P. G. McQueen, F. E. McKenzie, Age-structured red blood cell susceptibility and the dynamics of malaria infections. *Proc. Natl. Acad. Sci. U.S.A.* **101**, 9161–9166 (2004).
31. F. E. McKenzie, G. M. Jeffery, W. E. Collins, Plasmodium malariae blood-stage dynamics. *J. Parasitol.* **87**, 626–637 (2001).
32. F. E. McKenzie, G. M. Jeffery, W. E. Collins, Plasmodium vivax blood-stage dynamics. *J. Parasitol.* **88**, 521–535 (2002).
33. D. S. Hansen, Inflammatory responses associated with the induction of cerebral malaria: Lessons from experimental murine models. *PLoS Pathog.* **8**, e1003045 (2012).
34. P. Wilairatana, N. Tangpukdee, S. Krudsood, Definition of hyperparasitemia in severe falciparum malaria should be updated. *Asian Pac. J. Trop. Biomed.* **3**, 586 (2013).
35. T. King, T. Lamb, Interferon-γ: The Jekyll and Hyde of malaria. *PLoS Pathog.* **11**, e1005118 (2015).
36. J. Sellau *et al*., IL-22 dampens the T cell response in experimental malaria. *Sci. Rep.* **6**, 28058 (2016).
37. T. N. Shaw *et al*., Perivascular arrest of CD8+ T cells is a signature of experimental cerebral malaria. *PLoS Pathog.* **11**, e1005210 (2015).